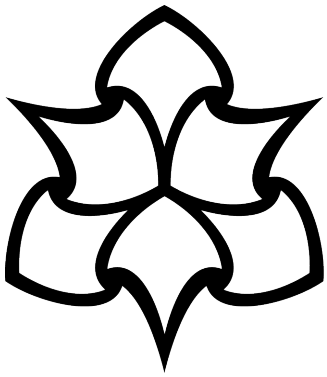

An Euler-Lagrange method considering bubble radial dynamics for modeling sonochemical reactors

Rashid Jamshidi*, Gunther Brenner

Institute of Applied Mechanics, Clausthal University of Technology, Adolph-Roemer Str. 2A, 38678 Clausthal-Zellerfeld, Germany

Abstract

Unsteady numerical computations are performed to investigate the flow field, wave propagation and the structure of bubbles in sonochemical reactors. The turbulent flow field is simulated using a two-equation Reynolds-Averaged Navier-Stokes (RANS) model. The distribution of the acoustic pressure is solved based on the Helmholtz equation using a finite volume method (FVM). The radial dynamics of a single bubble are considered by applying the Keller-Miksis equation to consider the compressibility of the liquid to the first order of acoustical Mach number. To investigate the structure of bubbles, a one-way coupling Euler-Lagrange approach is used to simulate the bulk medium and the bubbles as the dispersed phase. Drag, gravity, buoyancy, added mass, volume change and first Bjerknes forces are considered and their orders of magnitude are compared. To verify the implemented numerical algorithms, results for one and two-dimensional simplified test cases are compared with analytical solutions. The results show good agreement with experimental results for the relationship between the acoustic pressure amplitude and the volume fraction of the bubbles. The two-dimensional axi-symmetric results are in good agreement with experimentally observed structure of bubbles close to sonotrode.

Keywords: Sonochemical reactor, Bubble dynamics, Euler-Lagrange method, Keller-Miksis Equation

*Corresponding author. Tel.: +49 5323723715; fax: +49 5323722203
Email address : *rashid.jamshidi@tu – clausthal.de*

1. Introduction

Acoustic cavitation concerns the formation of bubbles from nuclei, their convection, oscillation and collapse [1]. These bubbles are responsible for dissipation of the acoustic energy in the liquid medium. Thus, determining the correct bubble distribution is an important goal in designing sonochemical reactors. The most important technological problem is upscaling the laboratory reactors to industrial scales ones in which the uniformity of the cavitational activity cannot be guaranteed. This uniformity, in addition, is disturbed due to external instruments such as aluminum foils and hydrophones during experimental investigations [2, 3]. Furthermore, the majority of experimental investigations are on the behavior of a single bubble during a short period of time such as the work of Lauterborn et al. [4] and Dangla and Poulain [5]. These experiments are of limited value to understand the state of a bubble swarm which is the most significant factor affecting the cavitational activity. Thus, to understand the design aspects of sonochemical reactors such as the dependency of the cavitational activity on the operating parameters and their optimum values [6], theoretical models as well as experimental investigations should be utilized [7].

Computational models may help in optimizing the geometry and operating parameters of a reactor. However, formulating a comprehensive physical model is still a challenge since not all of the phenomena are completely understood [8]. Furthermore, the disparity of the length and time scales causes severe mathematical problems. A majority of models dealing with bubbles in an acoustic field focus on a Rayleigh type equation for a single bubble during one or several acoustic periods [9, 10]. As a result the pressure and temperature at the bubble position during the oscillation and after its collapse are predictable. These parameters may help in estimating the optimum design parameters such as cavitational yield in a reactor [11]. Furthermore, the energy analysis of a single bubble dynamics could be helpful in determining the dissipation of power in the whole geometry of the reactor [12, 13]. However, predicting the heat and mass transfer as well as the chemical consequences at a microscopic scale in these models is still of challenge. Furthermore, the swarm behavior of bubbles can not be figured out from single bubble dynamics.

The second group of the models concerns the modeling of the cavitational activity by finding the acoustic pressure amplitude as a field quantity. In this category, the acoustic pressure is predicted without considering the effect of

bubbles [14] or by estimating their effect using simplifications [15, 16]. These approaches allow to determine the effect of parameters such as frequency and intensity of the ultrasound source or the boundaries, with respect to sound propagation and damping [17].

Most of the aforementioned references do not concentrate on the bulk medium motion. This flow field may be a result of external momentum sources, such as the inlet/outlet of a continuous feed reactor. Alternatively, they may be due to a strong acoustic source (acoustic streaming). Previous studies on the fluid motion in presence of a sound field are limited to investigate the acoustic streaming and are not for a combination with other momentum sources (see Ref. [18] or Ref. [19] and references therein). Furthermore, the experimental works in this field are usually conducted by considering some chemical characteristics such as mixing time of the reactants in a sonochemical reactor [20]. Since recent sonochemical reactors may be designed for reacting flows [21], the influence of external convective sources should also be considered. Besides that, it is important to understand the mixing and hydrodynamic characteristics due to the presence of solid/gas phases in a continuous feed reactor [22]. The idea of modeling of such a flow field is that it can help in placement of the reactants in zones of maximum cavitational intensity, flow distributors and near transducers for eliminating zones with weak cavitational activity [23].

Recently, hydrodynamic cavitation phenomena including the radial dynamics of externally driven bubbles are investigated by Abdel-Maksoud et al. [24]. However, due to the large difference between time scales of the oscillations of the bubbles and the bulk liquid flow, there are no attempts toward simultaneous modeling of these events using an Euler-Lagrange method in sonochemical reactors. The works of Parlitz et al. [25] and Mettin et al. [26] are some of the first attempts to use an Euler-Lagrange approach for the motion of bubbles under the action of ultrasound. By applying a particle model, they found that the primary Bjerknes force creates filaments of bubbles (streamers) due to the motion of the bubbles towards the nodes or antinodes of the acoustic field. Nevertheless, these works also suffer from the lack of investigating the external convective sources. Therefore, the present paper seeks to find a new method to investigate the motion of bubbles with varying radii and the formation of their quasi-steady structure under the action of a strong acoustic field.

2. Theory

2.1. Field quantities

For small amplitude waves, the distribution of the acoustic pressure may be described by the linear wave equation. Decomposing this equation into a spatially varying amplitude and a harmonic contribution, results to a Helmholtz type equation

$$\nabla^2 p + k^2 p = 0\,. \tag{1}$$

Here, $k = \omega/c$ denotes the wave number in which ω is the frequency of the wave, c is the speed of sound in the medium and p is the acoustic wave amplitude.

The motion of the turbulent, Newtonian, incompressible fluid may be governed by the RANS models, i.e., the convection equations for mass and momentum together with a transport model for the turbulent kinetic energy k and the turbulent dissipation rate ϵ. Here, the standard $k-\epsilon$ model is selected for turbulence modeling. Details of the model are not presented here. In the following, $\mathbf{U_f}$ denotes the fluid velocity.

2.2. Lagrangian approach for bubble motion

The motion of each individual bubble in a Lagrangian approach is governed by Newton's second law

$$m_b \frac{d\mathbf{U_b}}{dt} = \mathbf{F_G} + \mathbf{F_{AM}} + \mathbf{F_{vol}} + \mathbf{F_D} + \mathbf{F_{Bj1}}\,, \tag{2}$$

in which m_b is the mass of the bubble and $\mathbf{U_b}$ is its velocity. The Right Hand Side (RHS) of Eq. (2) contains the gravitational force $\mathbf{F_G} = (1 - \frac{\rho}{\rho_b}) m_b \mathbf{g}$, the added mass force $\mathbf{F_{AM}} = \frac{m_b \rho}{2\rho_b}(\frac{D\mathbf{U_f}}{Dt} - \frac{d\mathbf{U_b}}{dt})$, the volume variation force $\mathbf{F_{vol}} = \frac{\rho}{2\rho_b}\frac{dm_b}{dt}(\mathbf{U_f} - \mathbf{U_b})$ which represents momentum transfer due to changes in the bubble volume [27], the drag force and the primary Bjerknes force. In these equations, ρ_b is the density of the bubble that is mainly filled with gas such as air. The last two forces are explained in the following.

The drag force is a result of the relative motion between the bubble and the surrounding fluid and can be expressed as

$$\mathbf{F_D} = -m_b \frac{\mathbf{U_b} - \mathbf{U_f}}{\tau_b}\,, \tag{3}$$

where τ_b is the relaxation time for the bubble. The value of τ_b ,which represents the time for a bubble to respond to the changes in the local fluid velocity, can be obtained as

$$\tau_b = \begin{cases} \frac{\rho_b d_b^2}{18\mu} & : Re_b < 0.1 \\ \frac{4}{3}\frac{\rho_b d_b}{\rho C_D |\mathbf{U_f} - \mathbf{U_b}|} & : Re_b > 0.1 \end{cases}$$

in which d_b is the diameter of the spherical bubble, Re_b is the bubble Reynolds number defined based on the relative velocity between bubble and the surrounding fluid and the drag coefficient, C_D, is obtained from the Schiller and Naumann relation [28].

As the acoustic pressure is oscillatory in time, the average of the primary Bjerknes force on the bubble during one acoustic cycle is calculated as follows

$$\mathbf{F_{Bj1}} = -\langle V(t)\nabla p(t)\rangle_t \,, \tag{4}$$

where $V(t)$ is the volume of the bubble and $\nabla p(t)$ is the pressure gradient at the bubble position. The operator $\langle . \rangle_t$ denotes averaging in time.

2.2.1. Updating the bubble position

To find the new position of a bubble as $\mathbf{x}_b^{n+1} = \mathbf{x}_b^n + \mathbf{U}_b^{n+1} dt$, the updated bubble velocity $\mathbf{U}_b^{n+1}$ is obtained by substituting Eqs. (3) and (4) and the gravitational, added mass and volume variation forces into Eq. (2). To calculate drag, added mass and volume variation forces, the updated value for the bubble velocity is applied, that means a backward (implicit) Euler method is used. After some algebraic operations, the updated bubble velocity is obtained as below

$$\mathbf{U}_b^{n+1} = \frac{\mathbf{U}_b^n + \frac{2dt}{2\rho_b+\rho}\left((\rho_b - \rho)\mathbf{g} + (\frac{\rho}{2V_b}\frac{dV_b}{dt} + \frac{\rho_b}{\tau})\mathbf{U}_{@b} - \frac{1}{V_b}\langle V_b \nabla p(t)\rangle_t\right)}{1 + \frac{2dt}{2\rho_b+\rho}(\frac{\rho}{2V_b}\frac{dV_b}{dt} + \frac{\rho_b}{\tau})} \,, \tag{5}$$

in which $\mathbf{U}_{@b}$ is a new notation for $\mathbf{U_f}$ to show the velocity vector of the liquid at the bubble position. This vector is interpolated from the solution of the flow field at each time step.

2.3. Bubble dynamics

For the sake of simplicity, it is assumed that the spherical shape of the bubbles remains unchanged and the radial dynamics of a bubble including

the compressibility effects to the first order of acoustical Mach number, $\dot{R}/c$, is modeled by the Keller-Miksis Equation (KME) [29]

$$\rho\left((1-\frac{\dot{R}}{c})R\ddot{R}+\frac{3}{2}\dot{R}^2(1-\frac{\dot{R}}{3c})\right)=\left(1+\frac{\dot{R}}{c}+\frac{R}{c}\frac{d}{dt}\right)\left(p_g-\frac{2\sigma}{R}-\frac{4\mu\dot{R}}{R}-p\right)\,, \quad (6)$$

in which overdots denote differentiation with respect to time. Here, the pressure of the gas inside the bubble, p_g, is supposed to change adiabatically and p, the acoustic pressure at the location of the bubble center is defined as

$$p=p_0-p_a sin(\omega t)\,. \quad (7)$$

The linear theory of bubble oscillation leads to some approximate solutions for predicting the bubble behavior. Therefore, it is helpful in verifying the results of the numerical algorithms applied in CFD simulations. Linearization of the ordinary differential equation (ODE) for the bubble dynamics with the assumption of $R(t)=R_0+R'(t)$, leads to an inhomogeneous second order ODE as

$$\ddot{R}'+\beta\dot{R}'+\omega_0^2R'=-\frac{p_a}{\rho R_0}sin(\omega t)\,, \quad (8)$$

in which ω_0 and β are the resonant frequency of the bubble and the damping factor respectively published elsewhere [25].

The solution of Eq. (8) has the form of $R'(t)=R'_a sin(\omega t+\phi)$ in which the phase shift ϕ depends on the initial radius of the bubble and the frequency of the wave and R'_a is the amplitude of oscillations. The variation of bubble radius obtained from Eq. (6) and Eq. (8) is shown in Fig. 1. The results are compared for a pressure amplitude of p_a=10 kPa, ultrasound frequency of f=20 kHz and initial radius of R_0=5 μm in Fig. 1-b. The value of 10 kPa is adopted to check the validity of the linear theory, because this magnitude is about ten percent disturbance in an equilibrium pressure of 101 kPa.

It is clear that for this range of pressure amplitudes, the linear theory predicts the bubble behavior quite well. However, the solution of Eq. (6) in the case of p_a=120 kPa in Fig. 1-c, which is in the non-linear region, shows that the linear approximation is pointless. Therefore, the average values required for calculating the primary Bjerknes and volume variation forces must be obtained from Eq. (6) instead of Eq. (8). However, to verify the applied

method in the software, for some simple test cases the results of linear theory are mentioned and compared.

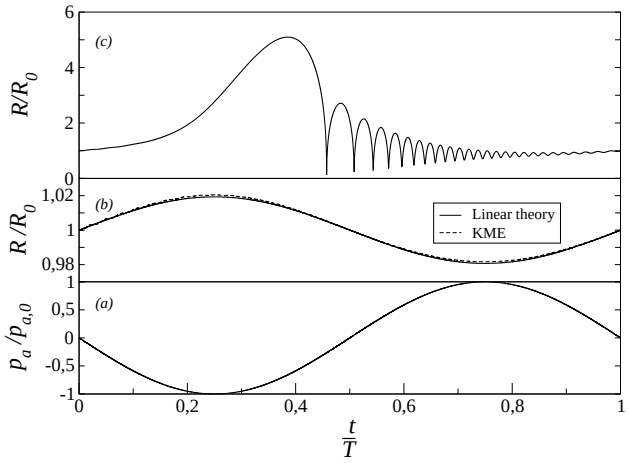

Figure 1: Variation of radius of a 5 μm bubble excited by a 20 kHz wave. (a): normalized acoustic pressure, (b): comparison between linear theory (Eq. (8)) and Eq. (6) for p_a=10 kPa and (c) Variation of bubble radius for p_a=120 kPa.

3. Numerical set-up

3.1. Procedure

All simulations are performed using OpenFOAM, a free software toolbox for continuum mechanics, specially for CFD. First, one and two dimensional (1D and 2D) computational domains are selected to verify the numerical method. The wave equation in the frequency domain, Eq. (1), is solved and the motion of a single bubble due to the primary Bjerknes force is investigated. Since a comparison with analytical solutions is of interest, the simulations are conducted for a pressure amplitude in the linear region. Thereafter, a flow field is added to the simulation for a 1D problem and a single bubble is investigated to be excited by acoustic pressure and convected by the flow. The convection causes the bubble to move along the streamline while the acoustic pressure amplitude as well as the radius of the bubble is changing. The radial motion of the bubble is investigated using Eq. (6). The result

is a relationship between acoustic pressure amplitude at each point and the volume of a single bubble. This relationship could be justified to find an equilibrium model for variation of the volume fraction of the bubbles and the acoustic pressure amplitude in sonochemical reactors. Previously, it was considered as a linear function [17, 30, 31]. The final step is applying the same procedure to a 2D reactor with a large number of bubbles and comparing the structure of bubbles with experiments [32].

3.2. Geometries, boundary conditions and physical properties

In sonochemical reactors used for mixing, the frequency of the ultrasonic wave is in the range of kHz [6, 33]. In the present work, the selected frequencies are about 20 kHz which is a common value for ultrasound transducers used in sonochemistry. The liquid is water in which the speed of sound is about 1500 m/s. Therefore, the wavelength of the wave approximately equals to 7.5 cm. The length of the 1D domain is 10 cm and for the 2D linear test case, a 10 cm$\times$10 cm square is considered. Hence, the produced standing wave can experience both nodes and antinodes. Schematics of the selected domains as well as the boundary conditions applied to them are presented in Fig. 2.

The boundary conditions for the flow field are prescribed values of velocity, turbulent kinetic energy and turbulent dissipation rate and zero gradient for the other parameters at the inlet. At the walls, the no slip boundary condition is imposed. The exit section is an outflow in which all gradients are set to zero except for the hydrodynamic pressure. Since the majority of experiments are conducted in stagnant liquids, the flow-field solver is only examined for a simple 1D case. Nonetheless, applying an external convection source is not a laborious task in OpenFOAM for the other test cases.

To solve the wave equation in the frequency domain, all the lateral walls of the geometries are supposed to absorb the ultrasound waves. Thus, they are modeled using Dirichlet type boundary condition with p =0 in the Helmholtz equation. In the 1D simulations, the left end of the domain is the ultrasound source which has a fixed pressure amplitude p_a=10 kPa for linear analysis and p_a=180 kPa for nonlinear investigation. The right end is set as a pressure release boundary, that is a Dirichlet boundary condition with p =0. For the first 2D simulation, the upper boundary has a fixed pressure amplitude p_a=10 kPa and the other ones are pressure release boundaries. For the second 2D case, the pressure amplitude is calculated from the external power applied to the sonotrode and physical and geometrical properties. In addition, the

free surface and the side walls are pressure release boundaries while the side of the sonotrode and the bottom wall are assumed to reflect the wave. Other physical properties required for the simulations are set as follows: the heat capacity ratio of the gas inside the bubble γ=1.4, the density of the gas inside the bubble ρ_b=1.2 kg/m^3, the surface tension σ=0.0725 N/m, the density of the liquid, ρ=1000 kg/m^3 and the viscosity of the liquid μ=0.001 Pa.s. Several simulations are conducted to check the grid independency of the results. Because of the simple geometrical configurations, the results of the wave equation and flow field were almost similar for different number of grid points. Finally, 10000 cells for the 1D test case and 200×200 cells for the first 2D geometry test case are adopted.

4. Results and discussion

4.1. Orders of magnitude of the forces

Assuming the displaced mass of the fluid by the bubble as ρV_b, the orders of magnitude of the forces on the RHS of Eq. (2) per displaced mass of the fluid are obtained as $|g|$ for the gravitational force, $\overline{U}/T_f$ for the inertia and the volume variation forces and $\nabla p_a/\rho$ for the primary Bjerknes force. For the drag force, this order is $\overline{U}\nu/d_b^2$ for $Re_b < 0.1$ and $\overline{U}^2/d_b$ for $Re_b > 0.1$. In these relations, $\overline{U}$ denotes the order of the velocity magnitude of the bubble and the bulk of the medium and T_f is the time scale of the flow field. For common sonochemical reactors, the nuclei of bubbles have the diameter of about 10^{-5}m. The reactors are normally filled with water as the bulk medium with $\nu = 10^{-6}$m^2/s and the mean velocity of the flow field and its time scale are in the order of 1 m/s and 10^{-2}s, respectively. Therefore, it can be observed that the drag force is much stronger than the other forces and depending on the gradient of the acoustic pressure, the primary Bjerknes force could also be of great importance. For small amplitude of acoustic pressure in which the linear theory is applicable, the primary Bjerknes force is also negligible. However, for high amplitudes in the nonlinear region, this force plays a substantial rule in determining the trajectories of the bubbles. As the effect of this force on the bubbles trajectories is of interest in the present study, the implementation of this force in the Lagrangian approach is examined first.

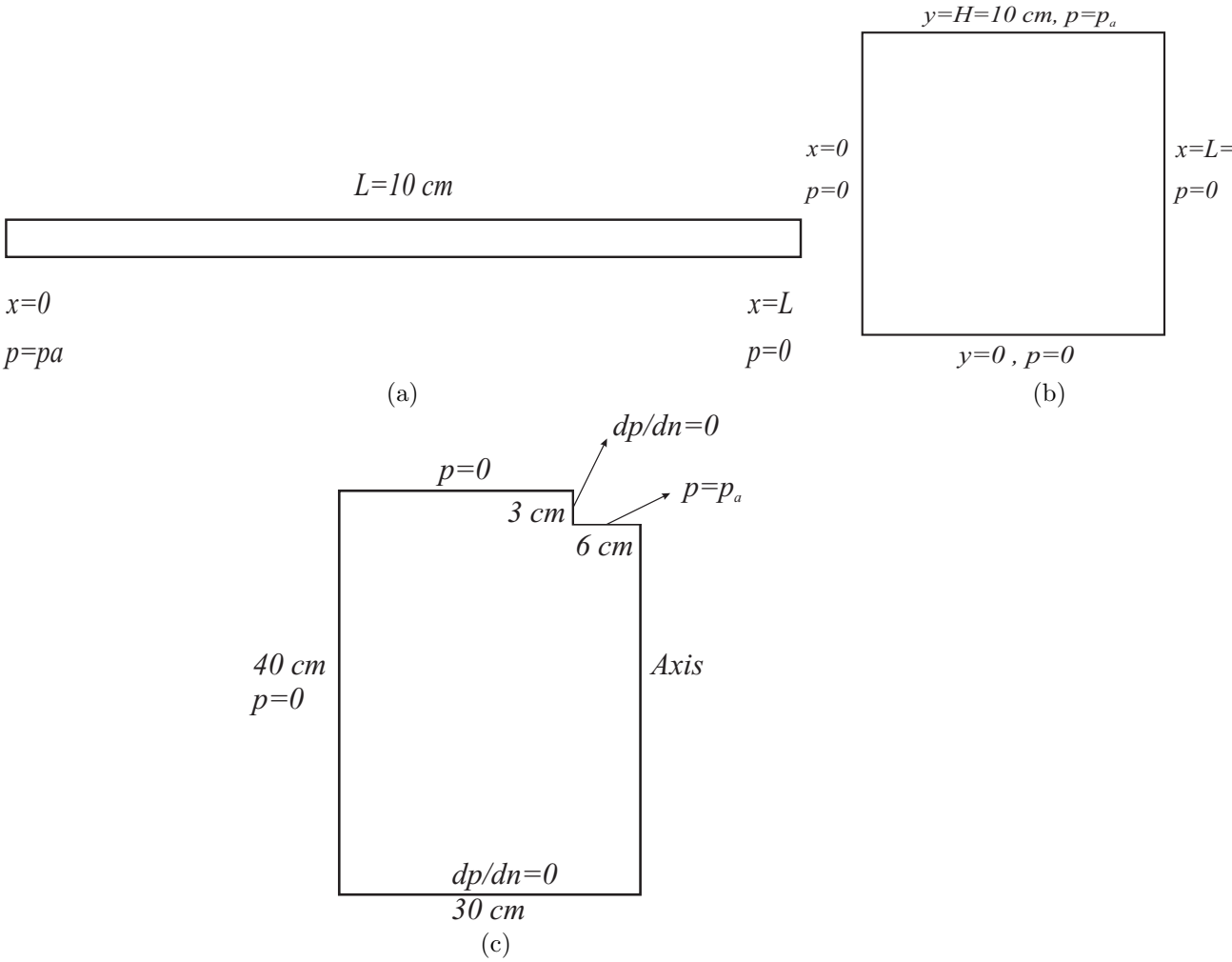

Figure 2: Geometries considered as the test cases with their boundary conditions and dimensions. (a): 1D, (b): 2D to be compared with analytical solution and (c): 2D to be compared with experiments.

4.2. One-dimensional simulation

4.2.1. Single bubble motion- Linear oscillations

In the case of an acoustic standing wave as $p(\mathbf{x},t) = p_0 - p_A(\mathbf{x})sin(\omega t)$, the average of the primary Bjerknes force during one acoustic cycle can be obtained as

$$\mathbf{F_{Bj1}} = -\frac{1}{2}V'\nabla p_A cos(\phi)\,, \tag{9}$$

in which $V' = 4\pi R_0^2 R'_a$ is the amplitude of the oscillation of the bubble volume [25]. According to Leighton [34], larger bubbles with initial radius bigger than the resonant radius ($cos(\phi)$ >0) are attracted towards the pressure nodes and smaller bubbles with $R_0 < R_{res}$ ($cos(\phi)$ <0) move towards the pressure antinodes. The resonant radius is the radius of the bubbles whose resonance frequency ω_0 is equal to the frequency of the external acoustic source ω .

Equation (1) in 1D reduces to $p'' + k^2 p = 0$ and with the boundary conditions illustrated in section 3.2, one can find a solution as $p_A(x) = p_a sin(k(l-x))/sin(kl)$, $k > 0$ and $kl \neq n\pi$ for the amplitude of the acoustic pressure and its gradient as $\nabla p_A(x) = -p_a k cos(k(l-x))/sin(kl)$. On the other hand, the solution of Eq. (8) leads to the following relationships for the amplitude of the linear oscillations and the phase shift

$$R'_a = \frac{p_A(x)}{\rho R_0 \sqrt{(\omega_0^2 - \omega^2)^2 + (\alpha\omega)^2}}\,, \tag{10}$$

and

$$cos(\phi) = \frac{\omega^2 - \omega_0^2}{\sqrt{(\omega_0^2 - \omega^2)^2 + (\alpha\omega)^2}}\,. \tag{11}$$

By applying these two relations in Eq. (9), the primary Bjerknes force at each point of the domain is obtained. Finally, the equation of motion for a single bubble under the action of this force can be obtained as

$$\ddot{x} + A \cdot sin(2k(l-x)) = 0\,, \tag{12}$$

where A is a constant which can be written as

$$A = \frac{3}{4}\frac{kp_a^2(\omega_0^2 - \omega^2)}{\rho\rho_b R_0^2 sin^2(kl)((\omega_0^2 - \omega^2)^2 + (\alpha\omega)^2)}\,. \tag{13}$$

In deriving Eq. (13), it is assumed that due to the small oscillations of the bubble radius, the mass of the gas inside the bubble remains constant. Equation (12) can be solved with the use of elliptic integrals or by a backward Euler method (the 4^{th} order Runge-Kutta method reduces to the Euler method for this ODE). Here, the backward Euler method is used to find the solution. The resonant radius of the bubbles with the external frequency of 20 kHz is equal to 0.15 mm. Hence, two different cases, one with a radius smaller and one with a radius larger than 0.15 mm are assumed. The bubbles with initial radii of 5 μm and 0.5 mm are placed at x/L=0.026 in the geometry of 1D model. Comparisons between numerical simulation and analytical solution for the motion of the bubble are shown in Fig. 3. The bubble with the initial radius of 5 μm starts to oscillate around the nearest antinode at x/L=0.0625; while the other one tries to move toward the nearest pressure node outside of the domain. If the boundary condition at x=0 is not defined in the model, the bubble starts to oscillate around a virtual point outside of the domain that is exactly located at the next node of the pressure field. Hence, a boundary condition is defined at x=0 in a manner that if a bubble reaches to this point, it will stick to the wall. This definition also has a physical meaning because the bubbles tend to stick to the wall due to the effect of cohesion. The oscillation of the bubble with 0.5 mm in radius around the nearest pressure node inside the domain is also investigated and confirmed. The variation of the position has the same trend as Fig. 3-a and is not repeated. As it can be seen from the results, the FVM predicts the position of the bubble precisely. It should be noted that in the FVM, the radius of the bubble is changing due to the solution of Eq. (6) at each time step and the primary Bjerknes force is obtained from Eq. (4) instead of Eq. (9). However, because the amplitude of the acoustic source is not significantly high, the amplitude of the oscillation of the radius is approximately 2 percent of the initial radius (Fig. 1-b). Therefore, the variation of the radius can not affect the RHS of Eq. (5) considerably.

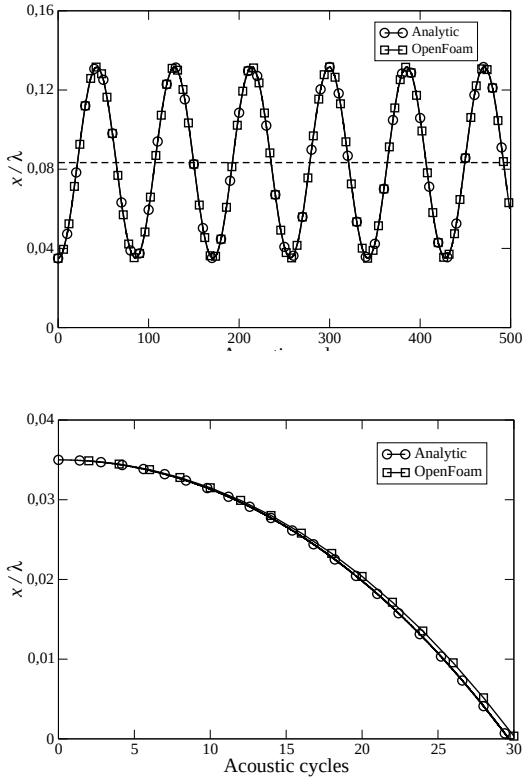

(b) $R_0 = 0.5\ mm$

Figure 3: Normalized position of the bubble due to the effect of primary Bjerknes force. Nondimensionalization is done by dividing the position to the wavelength of the wave, λ. (a): $R_0 = 5\ \mu m$ and (b): $R_0 = 0.5\ mm$. Dashed line shows the position of the nearest antinode.

4.2.2. Single bubble motion- nonlinear oscillations and convection

An inlet velocity of 10 m/s is applied to the model of section 4.2.1 to move the bubble from left to right. This value is adopted to ensure pushing the bubble to move along the domain without being hindered by the drag force. The drag force is the only force which is considered here to resist against the bubble motion due to the external convection source. If the Bjerknes force is activated, the bubble may oscillate around some specific points and is not able to experience all of the pressure amplitudes. The pressure amplitude at the inlet is set as 180 kPa to ensure the non-linear oscillation of the bubble. The initial diameter of the nuclei is 1.5 μm. Here, the goal is to find the local volume fraction of bubbles (total void volume occupied by the bubbles per unit volume) which is defined as

$$\beta = \frac{4\pi}{3} N R^3 \,. \tag{14}$$

Both N (number of bubbles) and R (their radius) are functions of pressure amplitude. In some references, the value of N is specified and assumed as a constant number, such as the works of Vanhille and Campos-Pozuelo [8] and Louisnard [35]. Moreover, some authors have assumed that if the pressure amplitude increases, the volume fraction of bubbles rises linearly [15]. The former assumption does not see the change of N due to creating children by the parent bubbles, even after violent collapse. In addition, the latter does not separate the contributions of N and R in increasing the value of β. Since the variation of R with respect to pressure amplitude can be derived in this work using the KME at each computational cell, only a linear function is assumed for changing the number of bubbles with pressure. It is supposed that after the collapse of a bubble at higher pressures, it is fragmented into smaller bubbles. The higher the value of the pressure, the higher the number of children produced by the initial nuclei. As the overall physical background is still unknown, here a linear function is applied and the method of its application is described as followings.

The maximum radius of the bubble in one acoustic period is calculated by Eq. (6) to find the volume of a single bubble at each point. It is assumed that a bubble requires a space equal to its maximum volume during one cycle. For a bubble with an initial diameter of 1.5 μm, the threshold of transient cavitation is p_a=184.5 kPa. At this pressure, the maximum radius of the bubble reaches to about 58 times of its initial radius (Fig. 4). Up to this point, as

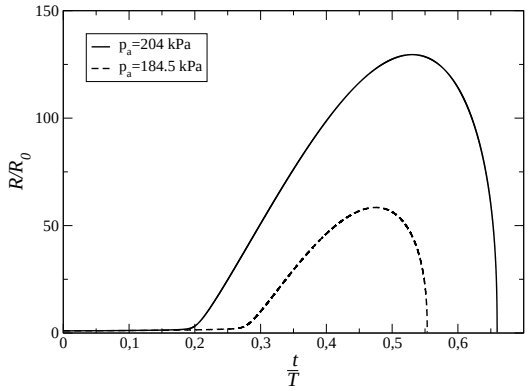

Figure 4: Collapse of a bubble with initial diameter of 1.5 μm for two different acoustic pressure amplitudes at frequency of 20 kHz.

the bubbles are oscillating almost linearly, their volume fraction is negligible and does not increase substantially with pressure. Thus, a small value of $\beta = 10^{-4}$ is considered for this pressure amplitude. This value is adopted since it is shown to have insignificant effect on wave propagation [15, 17]. By knowing this value and also the maximum volume of a single bubble, the number of bubbles per unit volume at the beginning of the transient cavitation region is estimated as 2.84×10^8. The same analysis can be done for a volume fraction of 10^{-1} as the upper limit for β and a pressure amplitude of p_a=204 kPa. The upper limit for β is adjusted because the damping of the ultrasonic wave for larger values does not allow the wave to propagate. In addition, the coalescence among bubbles at larger volume fractions will be dominant which leads to a so-called "saturated cavitation" phenomenon. The pressure amplitude of 204 kPa is adopted because it is observed in the experiment as the initial amplitude of the coalescence-dominated cavitation [36]. At this pressure, a bubble experiences a radius approximately 130 times of its initial radius (Fig. 4), that is $R_{max} = 97.5\ \mu m$. Therefore, a value of about 2.61×10^{10} is estimated for the number of bubbles per cubic meter. By conducting this analyses, a linear relationship is obtained between the number of bubbles and the pressure amplitude. This relationship as well as the variation of radius which is obtained from Eq. (6) can be applied to Eq.(14) to predict the volume fraction of bubbles. The final results can be compared with the experimental results from Akulichev [36] and are shown in Fig. 5 in which the volume fraction is plotted as a function of the pressure amplitude.

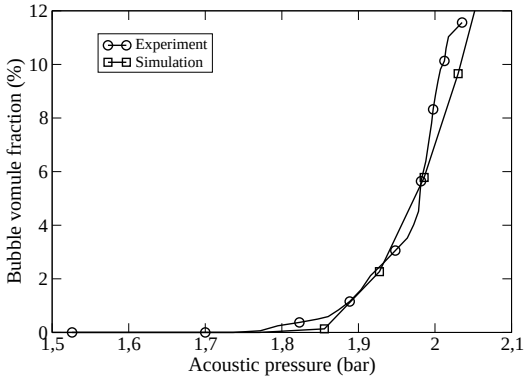

Figure 5: Comparison between experimental and numerical results for bubble volume fraction versus the pressure amplitude. Experimental data are from [36].

In the experiment, the volume fraction of bubbles is measured by inserting a capillary in the cavitation zone. The cavitation zone is located under a cylindrical ring transducer, exactly on the axis. The method measures the change of volume and is called dilatometric method (Rozenberg [37]). The result is a "quasi-steady" bubble density which could be used to calculate the volume fraction of bubbles. As can be seen from Fig. 5, after a threshold, transient collapse of bubbles occurs and their volume fraction increases sharply. As it is illustrated, the FVM results show good agreement in predicting the trend of bubble volume fraction as observed in experiments. It can be concluded that assuming a relation, even a linear one, between number of bubbles instead of their volume fraction and pressure amplitude leads to reasonable results. Nevertheless, the assumption made here could be modified by applying more sophisticated physical models on the population of bubbles in acoustic fields.

4.3. Two-dimensional simulation

4.3.1. Single bubble motion- Linear oscillations

In a 2D domain, Eq. (1) is written as $\partial^2 p/\partial x^2 + \partial^2 p/\partial y^2 + k^2 p = 0$. By applying the boundary conditions which are illustrated in section 3.2, the solution of this equation can be obtained by a Fourier series

$$p_A(x,y) = \sum_{n=1}^{\infty} \frac{4p_a}{n\pi sin\sqrt{k^2 - (\frac{n\pi}{l})^2}H} sin(\frac{n\pi x}{l}) sin\sqrt{k^2 - (\frac{n\pi}{l})^2}y\,. \qquad (15)$$

The gradient of this pressure distribution is substituted in Eq. (9). By assuming $c_n = n\pi/l$ and $d_n = \sqrt{k^2 - (n\pi/l)^2}$, the equations of motion for a single bubble under the action of the primary Bjerknes force can be written as

$$\ddot{x}_b + B \sum_{n=1}^{\infty} \frac{sinc_n x_b sind_n y_b}{n\pi sind_n H} \sum_{n=1}^{\infty} \frac{cosd_n x sind_n y_b}{l sind_n H} = 0\,, \tag{16}$$

and

$$\ddot{y}_b + B \sum_{n=1}^{\infty} \frac{sinc_n x_b sind_n y_b}{n\pi sind_n H} \sum_{n=1}^{\infty} \frac{sinc_n x_b d_n cosd_n y_b}{n\pi sind_n H} = 0\,, \tag{17}$$

where B is a constant as

$$B = \frac{24 p_a^2 (\omega_0^2 - \omega^2)}{\rho \rho_p R_0^2 ((\omega_0^2 - \omega^2)^2 + (\alpha\omega)^2)}\,. \tag{18}$$

The same assumptions as in the 1D case are applied in deriving these relations. Again, using a backward Euler method, Eqs. (16) and (17) are solved and the motion of a single bubble is compared to the results obtained by FVM simulation. A bubble with the initial radius of 5 μm is placed at x/L=0.5 and y/H=0.1 in the geometry of the 2D model (Fig. 2-b). The comparison between the numerical simulation and the analytical solution for the y-coordinate of the bubble position is shown in Fig. 6. It is observed that the bubble starts to oscillate around the nearest antinode at y/H=0.275. Because of the symmetricity of the pressure around the line x/L=0.5, the bubble does not move in x-direction. It is observed that the FVM gives reasonable results for the position of the bubble in the 2D test case.

4.3.2. Multiple bubbles motion- nonlinear oscillations

An axi-symmetric 2D geometry with 24000 cells is considered to reproduce the conical structure of bubbles in the vicinity of an ultrasound source, as observed in experiments [32]. In the experiment, a sonotrode with a diameter of 120 mm, a frequency of 20.7 kHz and an acoustic intensity (power per unit area of the sonotrode) of 8.2 W/cm^2 is placed in a tank. The tank made of glass walls is filled with water and has dimensions of 60 cm$\times$100 cm$\times$40 cm. The cone bubble structure is captured using a digital photo camera which focuses on the cavitation zone. Although the tank is cubic in

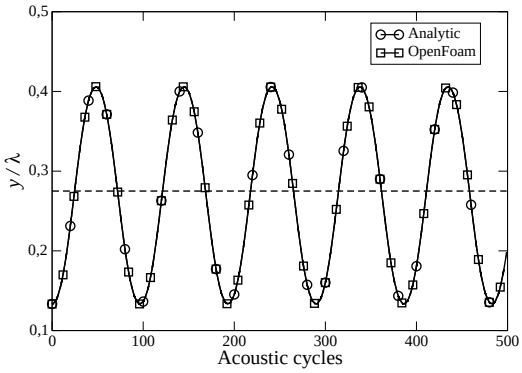

Figure 6: Normalized position of the bubble ($R_0 = 5\ \mu m$) due to the effect of primary Bjerknes force in 2D domain. The dashed line shows the position of the nearest antinode.

shape, assuming a cross section of a cylindrical tank in an axi-symmetric 2D geometry leads to reasonable result. The reason is the large dimension of the tank with respect to the smaller cylindrical sonotrode.

In order to apply the value of ultrasound power to the acoustic source in the simulations, the acoustic pressure amplitude in the simulation should be set as the boundary condition. This is done by the following relation [38]

$$p_{amp} = \sqrt{2\rho c I}\,, \tag{19}$$

in which I denotes the acoustic intensity. For the present configuration, the amplitude of pressure at the sonotrode is calculated as p_a=4.96 bar. 1200 bubbles with an initial radius of $R_0 = 2\ \mu m$ are distributed uniformly inside the axi-symmetric geometry in the vicinity of the sonotrode. The comparison between the results of simulation and the experimental observations is shown in Fig. 7. Although the bubbles show a chaotic unsteady motion, they accumulate around the pressure antinodes and also stick to the surface of the ultrasonic source as a quasi-steady structure. In addition, they are repelled from the pressure node and this leads to a conical shell with a highly populated base near the sonotrode, and a solitude zone inside the cone [35]. This trend is also observed in the present numerical simulations.

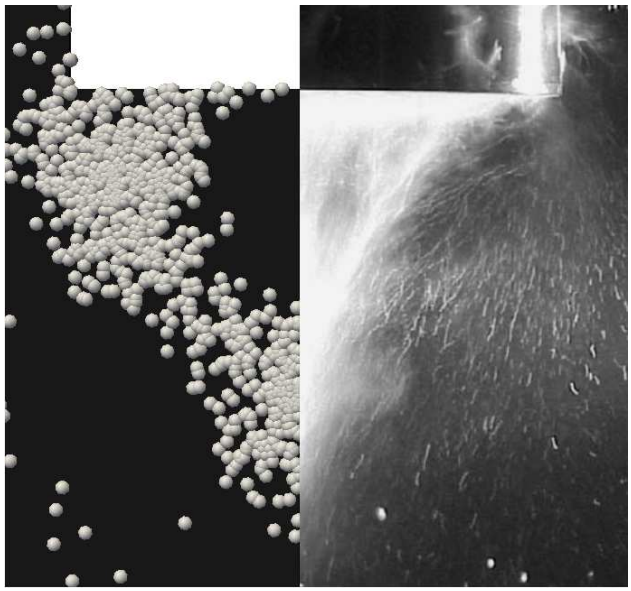

Figure 7: Conical structure of bubbles in the vicinity of ultrasonic horn. 1200 bubbles ($R_0 = 2$ μm) are located uniformly near the sonotrode in a axi-symmetric simulation (left). Right: reprinted from Ref. [32], with permission from Elsevier. Acoustic intensity=8.2 W/cm^2. frequency: 20.7 kHz.

5. Conclusions and Future works

The motion of cavitational bubbles under the action of ultrasonic pressure is investigated numerically including bubble radial dynamics. The summation of the forces on any individual bubble is calculated and with the use of the FVM, the velocities and positions of the bubbles are updated in a Lagrangian frame. To verify the implemented method in OpenFOAM, two benchmarks are considered and it is shown that the present approach, predicts the motion of the bubbles in a precise way. Since the radial dynamics of the bubbles undergoes complex variations in the case of high amplitudes of the acoustic source, the method is compared with experimental results in the nonlinear regime. Results show that the method can be applied to complex geometries with high number of nulcies to see the structure of bubbles inside sonochemical reactors. Moreover, the increment of the bubble volume fraction by increasing the acoustic pressure amplitude is verified. It is illustrated that by finding an appropriate relation for population of bubbles at different pressure amplitudes, the experimental results can be reproduced by

numerical simulations. The structure of bubbles in 2D simulation is also in agreement with experimental observations. It is depicted that in the case of high acoustic pressure amplitudes, the Bjerknes force is prevailing and dominates the formation of the conical structure.

References

[1] W. Lauterborn, C. D. Ohl, Cavitation bubble dynamics, Ultrasonics Sonochemistry 4 (1997) 65–75.

[2] V. S. Sutkar, P. R. Gogate, L. Csoka, Theoretical prediction of cavitational activity distribution in sonochemical reactors, Chemical Engineering Journal 158 (2010) 290 – 295.

[3] P. R. Gogate, P. A. Tatake, P. M.Kanthale, A. B.Pandit, Mapping of sonochemical reactors: Review, analysis, and experimental verification, AIChE Journal 48 (2002) 1542–1560.

[4] W. Lauterborn, T. Kurz, R. Geisler, D. Schanz, O. Lindau, Acoustic cavitation, bubble dynamics and sonoluminescence, Ultrasonics Sonochemistry 14 (2007) 484–491.

[5] R. Dangla, C. Poulain, When sound slows down bubbles, Physics of Fluids 22, doi: 10.1063/1.3415496 (2010) 041703–1,041703–4.

[6] B. Pohl, R. Jamshidi, G. Brenner, U. Peuker, Experimental study of continuous ultrasonic reactors for mixing and precipitation of nanoparticles, Chemical Engineering Science 69 (2012) 365–372.

[7] V. S. Sutkar, P. R. Gogate, Design aspects of sonochemical reactors: Techniques for understanding cavitational activity distribution and effect of operating parameters, Chemical Engineering Journal 155 (2009) 26–36.

[8] C. Vanhille, C. Campos-Pozuelo, Nonlinear ultrasonic waves: Two-dimensional simulations in bubbly liquids, Ultrasonics Sonochemistry 18 (2011) 679–682.

[9] P. R. Gogate, A. B. Pandit, Engineering design method for cavitational reactors: I. sonochemical reactors, AIChE journal 46 (2000) 372–379.

[10] C. Campos-Pozuelo, C. Granger, C. Vanhille, A. Moussatov, B. Dubus, Experimental and theoretical investigation of the mean acoustic pressure in the cavitation field, Ultrasonics Sonochemistry 12 (2005) 79–84.

[11] P. R. Gogate, A. Pandit, Sonochemical reactors: scale up aspects, Ultrasonics Sonochemistry 11 (2004) 105–117.

[12] O. Louisnard, A simple model of ultrasound propagation in a cavitating liquid. part i: Theory, nonlinear attenuation and traveling wave generation, Ultrasonics Sonochemistry 19 (2012) 56–65.

[13] N. P. Vichare, P. Senthilkumar, V. S. Moholkar, , P. R. Gogate, A. B. Pandit, Energy analysis in acoustic cavitation, Industrial and Engineering Chemistry Research 39 (2000) 1480–1486.

[14] S. Dähnke, F. J. Keil, Modeling of three-dimensional linear pressure field in sonochemical reactors with homogeneous and inhomogeneous density distribution of cavitation bubbles, Industrial and Engineering Chemistry Research 37 (1998) 848–864.

[15] S. W. Dähnke, F. J. Keil, Modeling of linear pressure field in sonochemical reactors considering an inhomogeneous density distribution of cavitation bubbles, Chemical Engineering Science 54 (1999) 2865–2872.

[16] S. Dähnke, F. Keil, Modeling of tsound fields in liquids with a nonhomogeneous distribution of cavitation bubbles as a basis for the design of sonochemical reactors, Chemical Engineering Technology 21 (1998) 873–877.

[17] R. Jamshidi, B. Pohl, U. A. Peuker, G. Brenner, Numerical investigation of sonochemical reactors considering the effect of inhomogeneous bubble clouds on ultrasonic wave propagation, Chemical Engineering Journal 189-190 (2012) 364–375.

[18] N. Riley, Acoustic streaming, Theoretical and Computational Fluid Dynamics 10 (1998) 349–356.

[19] S. Boluriaan, P. J. Morris, Acoustic streaming: from rayleigh to today, aeroacoustics 2 (2003) 255–292.

[20] N. P. Vichare, P. R. Gogate, V. Y. Dindore, A. B. Pandit, Mixing time analysis of a sonochemical reactor, Ultrasonics Sonochemistry 8 (2001) 23–33.

[21] H. Monnier, A. M. Wilhelm, H. Delmas, Effects of ultrasound on micromixing in flow cell, Chemical Engineering Science 55 (2000) 4009–4020.

[22] P. R. Gogate, V. S. Sutkar, A. B. Pandit, Sonochemical reactors: Important design and scale up considerations with a special emphasis on heterogeneous systems, Chemical Engineering Journal 166 (2011) 1066–1082.

[23] A. Kumar, P. R. Gogate, A. B. Pandit, Mapping of acoustic streaming in sonochemical reactors, Industrial and Engineering Chemistry Research 46 (2007) 4368–4373.

[24] M. Abdel-Maksoud, D. Hänel, U. Lantermanna, Modeling and computation of cavitation in vortical flow, International Journal of Heat and Fluid Flow 31 (2010) 1065–1074.

[25] U. Parlitz, R. Mettin, S. Luther, I. Akhatov, M. Voss, W. Lauterborn, Spatio-temporal dynamics of acoustic cavitation bubble clouds, Philosophical Transactions: Mathematical, Physical and Engineering Sciences 357 (1999) pp. 313–334.

[26] R. Mettin, S. Luther, C.-D. Ohl, W. Lauterborn, Acoustic cavitation structures and simulations by a particle model, Ultrasonics Sonochemistry 6 (1999) 25–29.

[27] E. Shams, J. Finn, S. V. Apte, A numerical scheme for euler-lagrange simulation of bubbly flows in complex systems, International Journal for Numerical Methods in Fluids 67 (2010) 1865–1898.

[28] L. Schiller, Z. Naumann, A drag coefficient correlation, Zeitschrift des Vereines Deutscher Ingenieure 77 (1935) 318.

[29] J. B. Keller, M. Miksis, Bubble oscillations of large amplitude, Journal of the Acoustical Society of America 68 (1980) 628–633.

[30] S. Dähnke, K. M. Swamy, F. J. Keil, Modeling of three-dimensional pressure fields in sonochemical reactors with an inhomogeneous density distribution of cavitation bubbles. comparison of theoretical and experimental results, Ultrasonics Sonochemistry 6 (1999) 31–41.

[31] G. Servant, J. Laborde, A. Hita, J. P. Caltagirone, A. Gerard, Spatio-temporal dynamics of cavitation bubble clouds in a low frequency reactor: comparison between theoretical and experimenatl results, Ultrasonics Sonochemistry 8 (2001) 163–174.

[32] A. Moussatov, C. Granger, B. Dubus, Cone-like bubble formation in ultrasonic cavitation field, Ultrasonics Sonochemistry 10 (2003) 191–195.

[33] P. R. Gogate, A. M. Wilhelm, A. B. Pandit, Some aspects of the design of sonochemical reactors, Ultrasonics Sonochemistry 10 (2003) 325–330.

[34] T. G. Leighton, The Acoustic Bubble, Academic press, London, 1994.

[35] O. Louisnard, A simple model of ultrasound propagation in a cavitating liquid. part ii: Primary bjerknes force and bubble structures, Ultrasonics Sonochemistry 19 (2012) 66–76.

[36] V. A. Akulichev, Experimental investigation of an elementary cavitation zone, Sov. Physc. Ac. 14 (1969) 284–289.

[37] L. D. Rozenberg, High-intensity ultrasonic fields, Plenum Press (1971), New York, NY.

[38] V. Raman, A. Abbas, S. C. Joshi, Mapping local cavitation events in high intensity ultrasound fields, in: proceeding of the COMSOL Users Conference, Bangalore, India (2006).